J Arid Land (2023) 15(5): 523–544
https://doi.org/ 10.1007/s40333-023-0059-7

Science Press Springer-Verlag

Propagation characteristics from meteorological drought to agricultural drought over the Heihe River Basin, Northwest China

BAI Miao[1,2], LI Zhanling[1,2,3*], HUO Pengying[1,2], WANG Jiawen[1,2], LI Zhanjie[4]

[1] School of Water Resources and Environment, China University of Geosciences, Beijing 100083, China;
[2] MOE Key Laboratory of Groundwater Circulation and Environmental Evolution, Beijing 100083, China;
[3] State Key Laboratory of Hydrology-Water Resources and Hydraulic Engineering, Nanjing Hydraulic Research Institute, Nanjing 210029, China;
[4] College of Water Sciences, Beijing Normal University, Beijing 100875, China

Abstract: In the context of global warming, drought events occur frequently. In order to better understanding the process and mechanism of drought occurrence and evolution, scholars have dedicated much attention on drought propagation, mainly focusing on drought propagation time and propagation probability. However, there are relatively few studies on the sensitivities of drought propagation to seasons and drought levels. Therefore, we took the Heihe River Basin (HRB) of Northwest China as the case study area to quantify the propagation time and propagation probability from meteorological drought to agricultural drought during the period of 1981–2020, and subsequently explore their sensitivities to seasons (irrigation and non-irrigation seasons) and drought levels. The correlation coefficient method and Copula-based interval conditional probability model were employed to determine the drought propagation time and propagation probability. The results determined the average drought propagation time as 8 months in the whole basin, which was reduced by 2 months (i.e., 6 months) on average during the irrigation season and prolonged by 2 months (i.e., 10 months) during the non-irrigation season. Propagation probability was sensitive to both seasons and drought levels, and the sensitivities had noticeable spatial differences in the whole basin. The propagation probability of agricultural drought at different levels generally increased with the meteorological drought levels for the upstream, midstream, and southern downstream regions of the HRB. Lesser agricultural droughts were more likely to be triggered during the irrigation season, while severer agricultural droughts were occurred mostly during the non-irrigation season. The research results are helpful to understand the characteristics of drought propagation and provide a scientific basis for the prevention and control of droughts. This study is of great significance for the rational planning of local water resources and maintaining good ecological environment in the HRB.

Keywords: meteorological drought; agricultural drought; drought propagation time; drought propagation probability; Copula function; interval conditional probability; Heihe River Basin

Citation: BAI Miao, LI Zhanling, HUO Pengying, WANG Jiawen, LI Zhanjie. 2023. Propagation characteristics from meteorological drought to agricultural drought over the Heihe River Basin, Northwest China. Journal of Arid Land, 15(5): 523–544. https://doi.org/10.1007/s40333-023-0059-7

*Corresponding author: LI Zhanling (E-mail: zhanling.li@cugb.edu.cn)
Received 2022-10-21; revised 2023-02-24; accepted 2023-02-28

1 Introduction

Drought has become one of the most common natural disasters worldwide (Mishra and Singh, 2012; Liu et al., 2018), typically inducing negative effects on the economy, agriculture, society, and environment (Cheng et al., 2013; Gu et al., 2020; Dahal et al., 2021; Zhang et al., 2022a). The economic losses caused by droughts during 1987–2006 in China accounted for more than 50% of meteorological disasters (Wang et al., 2012). It was estimated that under extreme drought conditions, the probability of corn yield reduction in Shandong Province of North China was greater than 80% and that in Jiangsu Province of East China was even greater than 86% (Zhang et al., 2022a). With global warming, drought assessment has become increasingly important for the establishment of drought prevention and early warning systems.

The American Meteorological Society classifies drought into four types: meteorological drought, agricultural drought, hydrological drought, and socioeconomic drought (Heim, 2002). Meteorological drought generally occurs earlier than hydrological drought and agricultural drought. Once meteorological drought happens, the other two drought types (hydrological drought and agricultural drought) can occur easily (Huang et al., 2015; Guo et al., 2020). Although there are differences in the occurrence time of droughts, the direct impact and disasters caused by droughts are often manifested through agricultural drought and hydrological drought (Guo et al., 2020; Zhou et al., 2021b). The propagation of water deficit signals between different types of droughts is defined as drought propagation (Apurv et al., 2017). Currently, research on drought propagation mainly focuses on propagation time, propagation probability, etc.

Drought propagation time is usually derived from the correlation analysis between two types of droughts (Abbas et al., 2021; Um et al., 2022). It is determined by the maximum correlation coefficient between a drought type on an n-month time scale and another drought type on a 1-month time scale; generally, the accumulation period n is defined as the drought propagation time (Li et al., 2016; Bayer Altin and Altin, 2021; Liu et al., 2021b; Xu et al., 2021). Based on the correlation method, some scholars found that propagation time from meteorological drought to agricultural drought in the Yellow River Basin was 0–3 months (Wang, 2020), and propagation time from meteorological drought to hydrological drought in the Pearl River Basin was 2–6 months (Zhou et al., 2021b), both in China. Significant spatial and temporal differences have also been determined in drought propagation time (Huang et al., 2017; Li et al., 2020; Xu et al., 2021; Zhou et al., 2021b). For example, Xu et al. (2021) evaluated propagation time from meteorological drought to agricultural drought and found that it gradually increased from 2 to 7 months from South to North China. Huang et al. (2017) concluded that propagation time from meteorological drought to hydrological drought had noticeably seasonal characteristics in the Weihe River Basin, China, with a shorter time in spring and summer, and a longer time in autumn and winter; while Li et al. (2020) determined a longer duration in spring and winter, and a shorter duration in summer and autumn in the upper Shaying River Basin, China. Ding et al. (2021) revealed that in North China, there was a stronger propagation relationship from agricultural drought to hydrological drought in summer and autumn compared to spring.

Drought propagation probability is generally determined by either conditional probability together with copula functions or by Bayesian network model (Shin et al., 2018; Sattar et al., 2019; Xu et al., 2019; Sun, 2021). Shin et al. (2018) employed the former method and found that propagation probability from meteorological drought to hydrological drought in Korea was 33% and 48%, based on standardized precipitation evapotranspiration index (SPEI) at the 3- and 6-month time scales, respectively. Sattar et al. (2019) used Bayesian network model to predict the propagation probability of hydrological drought triggered by meteorological drought in Korea and determined propagation probability to range from 27% to 60%. The propagation probability of different drought levels has attracted attention over the past few years. For example, Dehghani et al. (2019) found that extreme and severe meteorological drought led to hydrological drought with a 70% propagation probability in the Karun Basin of Iran, while other levels of meteorological drought resulted in a normal hydrological drought with less than a 50% propagation probability.

Jehanzaib and Kim (2020) employed Bayesian network model and Markov random fields to examine the propagation probability of meteorological drought and agricultural drought to hydrological drought in the Nakdong River Basin of Korea, and revealed that the joint propagation probability from severe and extreme meteorological drought and agricultural drought to severe and extreme hydrological drought ranged from 49% to 83% on average. Xu et al. (2021) concluded that the propagation probability of agricultural drought in China increased in parallel with the severity of meteorological drought. Zhu et al. (2021) detected the propagation probability of soil moisture drought to be on the rise in most regions across the globe with increasing meteorological drought levels.

The aforementioned studies have made progress in detecting drought propagation time and propagation probability across different regions; meanwhile, several scholars have also focused on the seasonal sensitivity of drought propagation time and the drought level sensitivity of propagation probability (e.g., Huang et al., 2017; Dehghani et al., 2019; Jehanzaib and Kim, 2020; Li et al., 2020; Ding et al., 2021; Xu et al., 2021; Zhu et al., 2021). However, further research is still required to enrich the study of drought propagation law, especially for drought propagation probability and its sensitivity to seasons and drought levels.

The Heihe River Basin (HRB) in Northwest China is characterized by sparse and concentrated precipitation and intense solar radiation, making the local drought problem prominent. Both drought and its propagation across the basin not only aggravate the local fragile ecological environment but also affect the water security, food security, and socio-economic development. Taking the HRB as the study area, this research aims to explore the propagation characteristics of drought propagation from meteorological drought to agricultural drought from two perspectives, namely, drought propagation time and propagation probability, and analyzes their sensitivities to seasons and drought levels. This work acts as a scientific basis for the management and planning of water resources in the HRB, and provides decision-making support in the early warning and prediction of droughts in this area.

2 Study area and data collection

2.1 Study area

The HRB, the second-largest inland river basin in Northwest China, is located in the arid zone of Northwest China (37°44′–42°40′N, 97°37′E–102°06′E). The basin has an area of 142,900 km^2, and can be divided into the upstream, midstream, and downstream regions from the south to north according to the locations of Yingluoxia and Zhengyixia hydrological stations (the hydrological stations at the outlets of the upstream and midstream of the HRB, respectively). The upstream region of the basin is the runoff producing area, and 90% of the water in the basin comes from the upstream (Wang, 2019). The midstream region is a runoff utilization area and is one of the top 10 commodity grain bases in China. The cultivated land area accounts for nearly 20% of the total area of the midstream region. It is also the essential ecological safety barrier and transportation hub along the Silk Road Economic Belt. The downstream region is a runoff consumption area with a vulnerable ecological environment.

The multi-year average annual precipitation and air temperature over the basin is 122.0 mm and 5.1°C, respectively, which were estimated from the observed data at gauge stations of the basin from 1981 to 2015 via the Thiessen polygon method. Precipitation gradually decreases from the upstream region to the downstream region, while air temperature increases from the upstream region to the downstream region. Due to climatic characteristics and water intake for irrigation in the midstream region, the downstream region usually suffers from droughts and water shortages (Feng and Su, 2020), which makes the ecological environment of Ejina Oasis, a national ecological reserve in China, more fragile. Topographically, the upstream region has high elevations, with peaks above 4000 m. The midstream region is relatively flat with elevations from 1200 to 2000 m, and the downstream region is open and flat with elevations below 1200 m (Fig. 1).

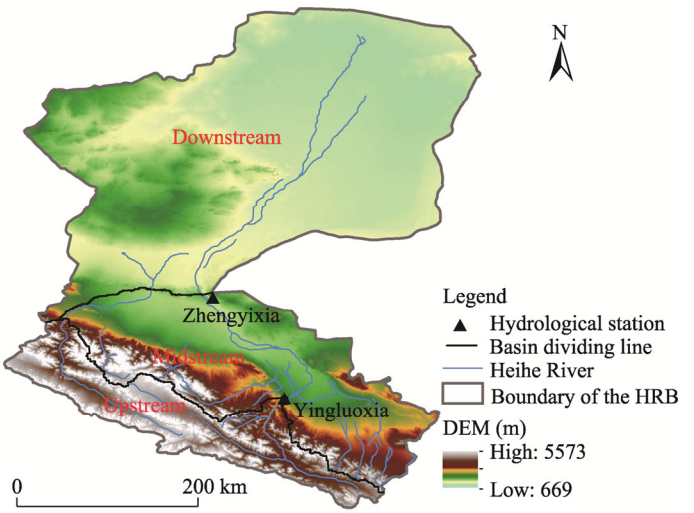

Fig. 1 Overview of the Heihe River Basin (HRB) and locations of hydrological stations. Black solid line is the basin dividing line of the upstream, midstream, and downstream. DEM, digital elevation model.

2.2 Global land data assimilation system (GLDAS)

GLDAS is a joint development of NASA's Gotha Space Flight Center and NOAA's National Center for Environmental Prediction, aiming to simulate land surface fluxes and storage of water and energy (Rodell et al., 2004). The GLDAS has been updated to version 2 (GLDAS-2), which includes 3-h, daily, and monthly products with spatial scales of 0.25° and 1.0° (https://earthdata.nasa.gov/). GLDAS-2 also comprises the versions of GLDAS-2.0 and GLDAS-2.1, in which the former covers the period of 1948–2014 and the latter covers the period of 2000–2020. Since both GLDAS-2.0 and GLDAS-2.1 involve the dataset from 2000 to 2014, we took the variable of precipitation as an example and compared the overlapping portion of the data in the HRB (Fig. 2). It is clear that the two curves representing each version are essentially consistent, with only slight differences in the extremes of individual years. Thus, the two datasets are largely comparable and consistent. Therefore, the data from GLDAS-2.0 during the period of 1981–1999 and the data from GLDAS-2.1 during the period of 2000–2020 were used in our study.

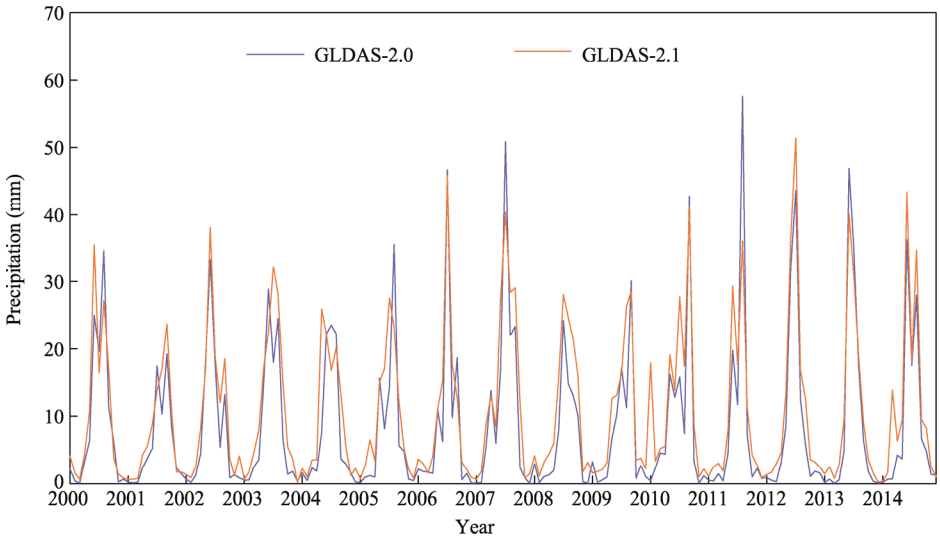

Fig. 2 Comparison of precipitation data derived from GLDAS-2.0 and GLDAS-2.1 during the period of 2000–2014. GLDAS, Global land data assimilation system.

There are inevitably some uncertainties involved in GLDAS datasets (e.g., Liu et al., 2021a; Wu et al., 2021; Zhang et al., 2021a; Zhou et al., 2021a). For example, Wu et al. (2021) found that GLDAS-2.1 slightly underestimated the climatology values in northern China, and slightly overestimated the values during summer and autumn in southern China. However, GLDAS-2 provides us with a substantial amount of available research data, particularly in areas where measured data are scarce. Several studies verified the reliability of GLDAS-2 dataset in specific regions. For example, Liu et al. (2019) used the Noah products from 1982 to 2015 in GLDAS-2.1 to investigate the spatial-temporal characteristics of the dry-wet regime and vegetation dynamic responses in the Yarlung Zangbo River Basin in China, and showed that the spatial-temporal patterns of precipitation and air temperature simulated by GLDAS-Noah fitted well with those of the *in-situ* data. Li et al. (2022) used the Noah products in GLDAS-2.1 to investigate the vegetation dynamic variations and their associated responses to environmental changes in the Yarlung Zangbo River Basin. Zhu et al. (2021) compared the GLDAS-2.0 data with observed data from global sites, and found that the data from GLDAS-2.0 were objective and reasonable for global drought propagation analysis. In order to assess the applicability of GLDAS-2 data in our study, we compared the precipitation and air temperature data derived from both GLDAS-2 and gauge stations of the HRB over the same period (1981–2015). Results show that GLDAS-2 data was essentially consistent with the observed data based on spatial trends; the performance of GLDAS-2 data was better on the regional average scale, although precipitation and air temperature in the upstream region were underestimated. Therefore, GLDAS-2.0 and GLDAS-2.1 data were selected as the basic data for our analysis.

More specifically, data of precipitation, air temperature, and soil moisture from 1981 to 2020 provided by Noah land surface model (Noah-LSM) in GLDAS-2.0 and GLDAS-2.1 (https://earthdata.nasa.gov/) were selected as our data sources. Table 1 reports the key information of these data. Soil moisture data include values at the depths of 0–10, 10–40, and 40–100 cm. The data were pre-processed prior to the drought analysis, including re-projection, conversion of units, etc. Figure 3a–c presents the spatial distribution of precipitation, air temperature, and soil moisture on the multi-year average scale. We then calculated the drought index based on the processed data (Vicente-Serrano et al., 2010; Martínez-Fernández et al., 2015). In addition, land use and land cover change data in 2015 were provided by Landsat 8 (https://landsat.gsfc.nasa.gov/satellites/landsat-8/). According to the current land use classification (Ministry of Agriculture of the People's Republic of China, 2017), there are 23 types of land use and land cover in the HRB, including forest, low-coverage grassland, cultivated land, desert, Gobi, etc. The distribution of each land use and land cover type is shown in Figure 3d.

Table 1 Key information of the data used in this study

Data	Unit	Spatial and temporal scales	Data source
Precipitation	kg/(m^2•s^2)	0.25°×0.25° Monthly	https://earthdata.nasa.gov/
Air temperature	K		
Soil moisture	kg/m^2		
Land use and land cover change	/	30 m	https://landsat.gsfc.nasa.gov/satellites/landsat-8/

Note: "/" denotes dimensionless.

3 Methods

3.1 Framework

This research aims to explore the propagation time and propagation probability of meteorological drought to agricultural drought over the HRB. Regarding drought propagation time, besides its seasonal sensitivity, the dynamic characteristics were also considered since propagation time may not remain stable owing to the effects of climate change and human activities (Liu et al., 2021b).

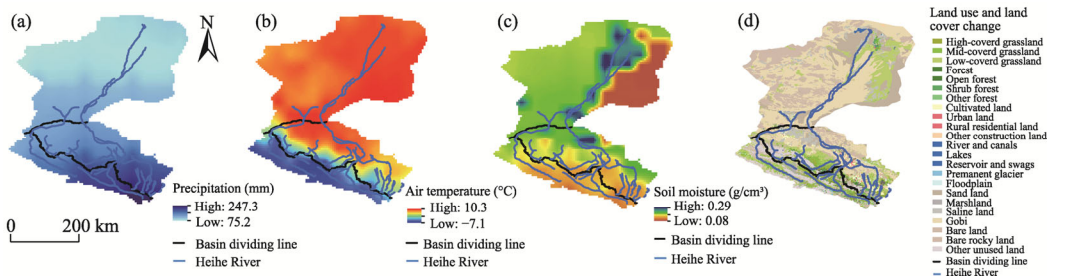

Fig. 3 Spatial distributions of multi-year average annual precipitation (a), annual average air temperature (b), soil moisture (c), and land use and land cover change (d) in the HRB

In terms of drought propagation probability, both seasonal sensitivity and drought level sensitivity (i.e., the probabilities of agricultural drought at different levels triggered by meteorological drought at different levels) were investigated.

The framework of this paper is presented in Figure 4. In particular, we focus on the following three issues: (1) the spatial characteristics of meteorological drought and agricultural drought across the basin from 1981 to 2020; (2) the seasonal sensitivity and dynamic characteristics of drought propagation time; and (3) both the seasonal sensitivity and drought level sensitivity of drought propagation probability.

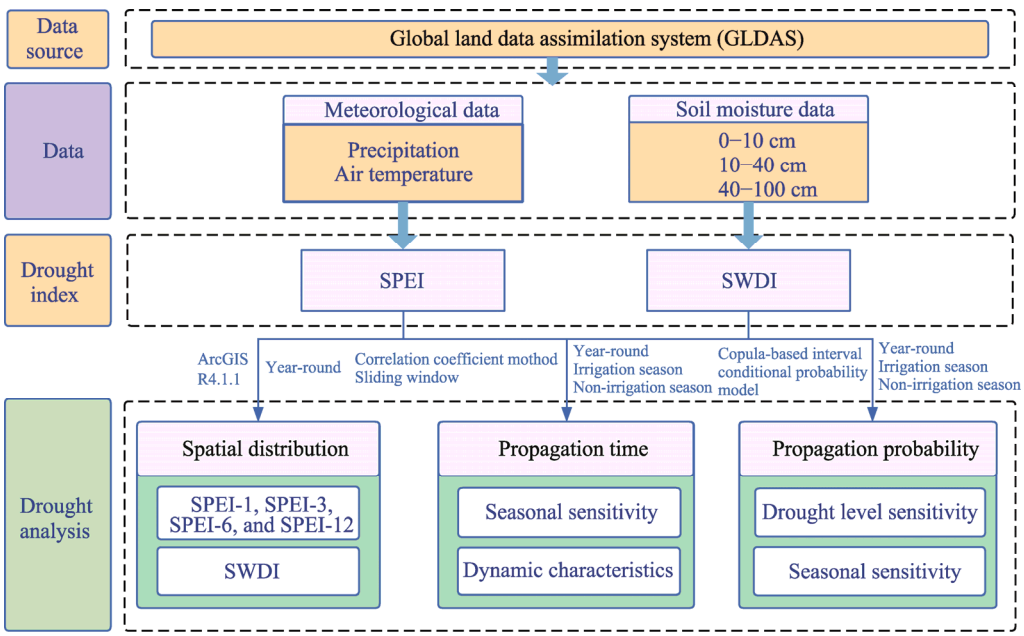

Fig. 4 Framework of this study. SPEI, standardized precipitation evapotranspiration index; SWDI, soil water deficit index. SPEI-1, SPEI-3, SPEI-6, and SPEI-12 mean SPEI at the 1-, 3-, 6-, 12-month time scales, respectively.

Meteorological drought and agricultural drought were characterized by SPEI and soil water deficit index (SWDI), respectively. As SPEI has the characteristics of multiple time scales, we used SPEI at the 1-, 3-, 6-, and 12-month time scales (denoted as SPEI-1, SPEI-3, SPEI-6, and SPEI-12, respectively) to investigate the spatial patterns of meteorological drought. The seasonal sensitivity and dynamic characteristics of drought propagation time were evaluated using the correlation coefficient method, sliding windows, and Mann-Kendall test. Propagation probability and its sensitivities to seasons and drought levels were quantified by the Copula-based interval conditional probability model. All data used here were from GLDAS-2.0 and GLDAS-2.1.

Unlike the regular four seasons in one year (spring, summer, autumn, and winter), we only consider the following two seasons in this study due to the high frequency of irrigation in the study area: (1) the irrigation season from April to September; and (2) the non-irrigation season from October to March of the following year.

3.2 Drought indices

3.2.1 Standardized precipitation evapotranspiration index (SPEI)

SPEI, proposed by Vicente-Serrano et al. (2010), is a drought index based on the standardized precipitation index (SPI) by introducing potential evapotranspiration. The Thornthwaite approach, which requires only monthly precipitation and air temperature data, is suggested to calculate the potential evapotranspiration (Li et al., 2016). SPEI is obtained after normalization by Equations 1 and 2:

$$\mathrm{SPEI} = \omega - \frac{c_0 + c_1\omega + c_2\omega^2}{1 + d_1\omega + d_2\omega^2 + d_3\omega^3}, \tag{1}$$

$$\omega = \sqrt{-2\ln F(D)} \quad (0 < F(D) \le 0.5), \tag{2}$$

where ω is the function of $F(D)$, and $F(D)$ is the probability distribution function of D, which is the difference series between precipitation and potential evapotranspiration; and c_0, c_1, c_2, d_1, d_2, and d_3 are constants, with the values of 2.515517, 0802853, 0.010328, 1.432788, 0.189269, and 0.001308, respectively. Further details of the calculation process can be found in Vicente-Serrano et al. (2010). Table 2 shows the classification of meteorological drought categories according to SPEI values.

Table 2 Classification of meteorological drought categories based on standardized precipitation evapotranspiration index (SPEI)

Level	Meteorological drought category	SPEI values
0	Non-drought	SPEI> –0.5
1	Mild drought	–1.0<SPEI≤ –0.5
2	Moderate drought	–1.5<SPEI≤ –1.0
3	Severe drought	–2.0<SPEI≤ –1.5
4	Extreme drought	SPEI≤ –2.0

3.2.2 Soil water deficit index (SWDI)

Unlike many drought indices based on meteorological variables or water balance equations, SWDI is based on a previous water deficit index (Martínez-Fernández et al., 2015). It considers the relationship between plant physiological state and soil moisture, and is more suitable for monitoring agricultural drought compared to other indices (Zhu et al., 2019; Wu et al., 2020). SWDI is calculated as follows:

$$\mathrm{SWDI} = \left(\frac{\theta - \theta_{\mathrm{FC}}}{\theta_{\mathrm{AWC}}}\right) \times 10, \tag{3}$$

$$\theta_{\mathrm{AWC}} = \theta_{\mathrm{FC}} - \theta_{\mathrm{WP}}, \tag{4}$$

where θ is the soil moisture (g/cm^3); and θ_{FC}, θ_{WP} and θ_{AWC} represent the field capacity (g/cm^3), wilting point (g/cm^3), and available water capacity (g/cm^3), respectively. The long-term minimum and maximum values based on the soil moisture time series are estimators of θ_{FC} and θ_{WP}, respectively (Bai et al., 2018).

Table 3 lists the agricultural drought categories based on the values of SWDI (Martínez-Fernández et al., 2015).

Table 3 Classification of agricultural drought categories based on soil water deficit index (SWDI)

Level	Agricultural drought category	SWDI values
0	Non-drought	SWDI>0
1	Mild drought	–2<SWDI≤0
2	Moderate drought	–5<SWDI≤ –2
3	Severe drought	–10<SWDI≤ –5
4	Extreme drought	SWDI≤ –10

3.3 Determination of drought propagation time

3.3.1 Pearson correlation coefficient

Propagation time can be defined as the time from the onset of meteorological drought to the beginning of agricultural drought, and can be simplified into a mathematical linkage between SPEI and SWDI in different accumulation periods. The time scale for meteorological drought is n months (n=1, 2, …, 12), while the time scale for agricultural drought is 1 month. The maximum Pearson correlation coefficient between SPEI-n and SWDI-1 represents the connection between meteorological drought and agricultural drought, and the accumulation period n is defined as the drought propagation time (Xu et al., 2021).

3.3.2 Mann-Kendall test and sliding windows

The Mann-Kendall test is a nonparametric statistical test used to quantitatively detect any significant trends in long term series. It does not require samples to follow a certain distribution and is less affected by outliers; thus, the Mann-Kendall test has been widely used in trend and mutation testing in the fields of hydrology and meteorology (e.g., Sun, 2021). The Sen's slope estimator is often used together with the Mann-Kendall test to quantify the magnitude of change. In particular, the Mann-Kendall test is applied to test the direction of the trend, while the Sen's slope estimator is employed to determine the magnitude of the trend (Bazrafshan, 2017; Moral et al., 2017).

The sliding window algorithm includes two important elements: the sliding distance and window length. By assigning these two element values, the new series is taken in a certain direction according to a fixed sliding distance and length (Shao et al., 2019). In this study, the sliding distance was set as 1 a and the sliding window was set as 20 a. Based on these settings, we divided the index series from 1981 to 2020 into 21 new series, and the dynamic changes of drought propagation time were then determined by calculating the values of the Sen's slope estimator for these 21 series.

3.4 Copula function and conditional probability

There are two commonly used Copula functions: Archimedean Copula and Elliptical Copula (Sun, 2021). The Archimedean Copula is highly representative and easy to construct, while the Elliptical Copula can establish non-normal relationships and better describe extreme events. The Copula function is calculated as follows:

$$C(F_1(u), F_2(v)) = F^{-1}(F_1(u), F_2(v)), \quad (5)$$

where $C(F_1(u), F_2(v))$ is the Copula function combined with two random variables u and v; F denotes the marginal distribution function; and F_1 and F_2 represent the marginal distribution functions of the two random variables, respectively.

Five Copula functions (including four Archimedean Copula functions and one Elliptical Copula function) were selected to establish the joint distribution of the meteorological drought and agricultural drought indices. Table 4 details their formulas and parameters. The Akaike information criterion (AIC) and Bayesian information criterion (BIC) were used to evaluate the goodness-of-fit of the functions. The Copula function with the smallest AIC or BIC value is considered as the best-fit function for the SPEI and SWDI series. Before establishing the Copula function, five alternative marginal distribution functions (i.e., normal, logistic, Weibull, general

extreme value (GEV), and Pearson-III (P3)) were chosen to fit the SPEI and SWDI series. The Kolmogorov-Smirnov (K-S) test was used to evaluate the performance of each marginal distribution function.

Table 4 Cumulative density functions and parameter ranges of Copula functions

Copula function type		$C(u, v)$	r value range
Archimedean Copula	Clayton	$(u^{-r}+v^{-r}-1)^{-\frac{1}{r}}$	$r>0$
	Gumbel	$\exp(-((-\ln u)^r+(-\ln v)^r)^{\frac{1}{r}})$	$r\geq 1$
	Frank	$-\frac{1}{r}\ln\left(\frac{(e^{-ru}-1)(e^{-rv}-1)}{e^{-r}-1}\right)$	$r\neq 0$
	Joe	$1-((1-u)^r+(1-v)^r-(1-u)^r(1-v)^r)^{\frac{1}{r}}$	$r\geq 1$
Elliptical Copula	t	$\int_{-\infty}^{t_k^{-1}(u)}\int_{-\infty}^{t_k^{-1}(v)}\frac{1}{2\pi\sqrt{1-r^2}}\exp[1+\frac{s^2-2rst+t^2}{k(1-r^2)}]^{-\frac{k+2}{2}}\mathrm{d}s\mathrm{d}t$	$r>0$

Note: u and v are two variables; r is the parameter; t_k^{-1} is the inverse function of the univariate t distribution function with a degree of freedom of k; and s and t are the univariate t distribution functions of variables u and v.

An interval conditional probability model can characterize the relationship between conditionally restricted random variables (Sattar et al., 2019). The interval conditional probability models of SPEI and SWDI were used to explore the probability of different levels of agricultural drought caused by different levels of meteorological drought. The corresponding formulas are described as:

$$\begin{aligned} P(v_1\leq V\leq v_2\,|\,u_1\leq U\leq u_2) &= \frac{P(v_1\leq V\leq v_2, u_1\leq U\leq u_2)}{P(u_1\leq U\leq u_2)} \\ &= \frac{C(F_1(u_1),F_2(v_1))-C(F_1(u_1),F_2(v_2))-C(F_1(u_2),F_2(v_1))+C(F_1(u_2),F_2(v_2))}{F_1(u_2)-F_1(u_1)}, \end{aligned} \tag{6}$$

where P is the conditional probability value; U and V represent the SPEI and SWDI series, respectively; v_1 and u_1 are the lower limits of variables v and u, respectively; v_2 and u_2 are the upper limits of variables v and u, respectively; F_1 and F_2 represent the marginal distribution functions of variables u and v, respectively; and $C(F_1(u_1), F_2(v_1))$, $C(F_1(u_1), F_2(v_2))$, $C(F_1(u_2), F_2(v_1))$, and $C(F_1(u_2), F_2(v_2))$ are the corresponding Copula functions.

4 Results

4.1 Meteorological drought and agricultural drought over the study area

Figure 5a–d show the spatial distribution of multi-year average meteorological drought based on SPEI over the HRB at different time scales from 1981 to 2020. The study area was generally dominated by the non-drought category at the multi-year average scale, although SPEI values differed with time scales. Larger SPEI values were observed based on SPEI-1 (mainly in green and yellow colors) with only 1% negative values, while smaller values were observed based on SPEI-3, SPEI-6, and SPEI-12 (mainly in orange and red colors), exhibiting much more negative values (37%, 31%, and 25% of the total values, respectively).

Figure 5e exhibits the spatial distribution of agricultural drought characterized by SWDI. The blue and green colors indicate non-drought with SWDI values greater than zero, while the yellow and red colors indicate drought with SWDI values lower than zero. With the exception of the river system and its surroundings in the midstream and downstream regions, the majority of the study area was dominated by orange, light green, and red colors, indicating the presence of agricultural drought in these regions. Extreme agricultural drought was detected in the eastern downstream region (red color in Fig. 5e), which is probably related to the low soil moisture in this region (Fig.

3c). Extreme agricultural drought was also detected in some upstream regions (orange color in Fig. 5e), although the intensity was not as severe as those in the eastern downstream region. The river system and its surrounding areas (blue color in Fig. 5e) were categorized as non-drought, which may be related to the high soil moisture.

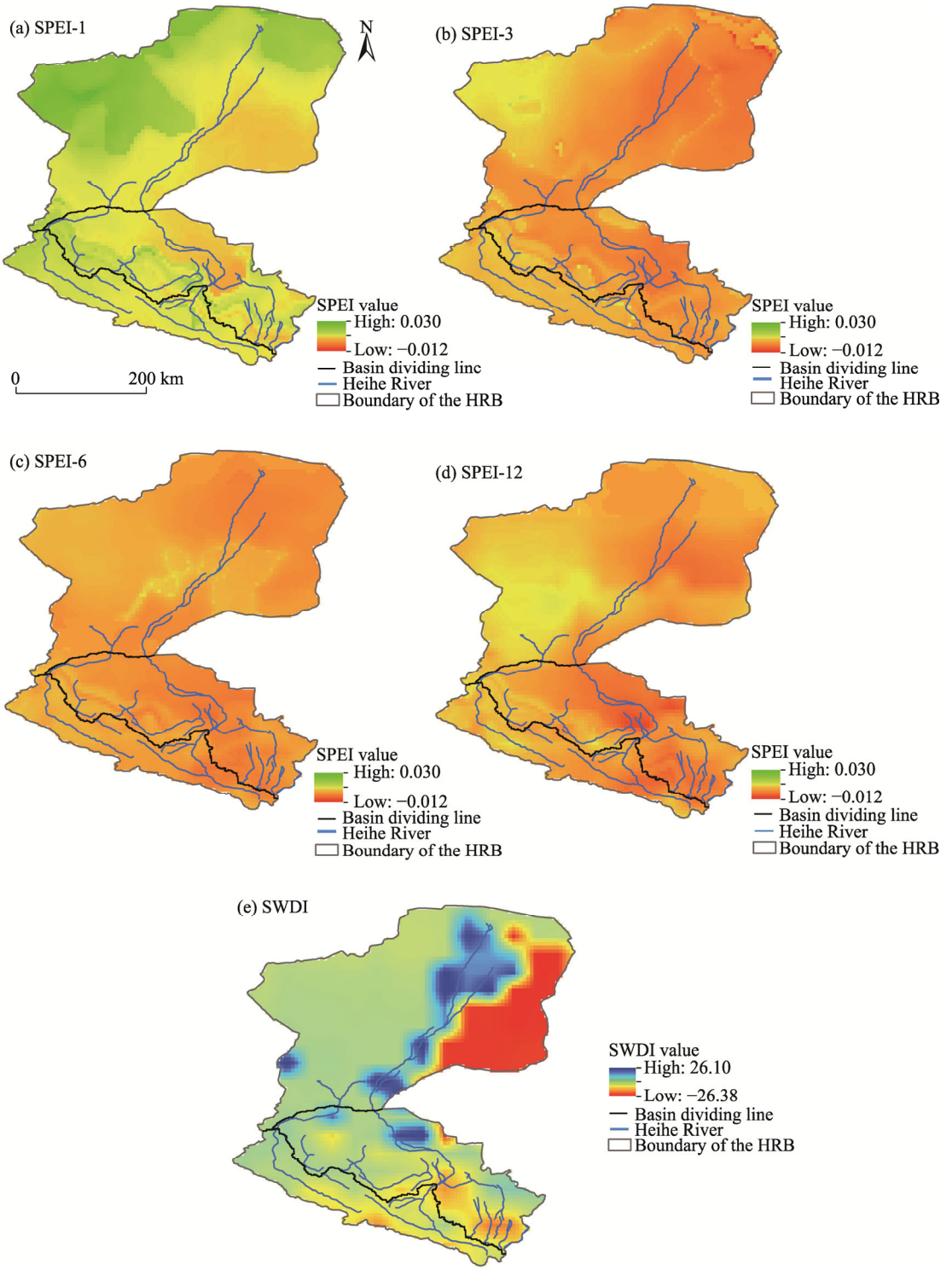

Fig. 5 Spatial distributions of SPEI-1 (a), SPEI-3 (b), SPEI-6 (c), SPEI-12 (d), and SWDI (e) in the HRB

4.2 Drought propagation time

4.2.1 Drought propagation time and its seasonal sensitivity

Figure 6 shows the spatial distribution of drought propagation time for the year-round, irrigation season, and non-irrigation season in the HRB. The redder the color tone, the longer the drought propagation time. Drought propagation time was observed to vary in different regions of the basin. Taking the case of Figure 6a as an example, the midstream and southern downstream regions experienced a short drought propagation time (less than 2 months), while other regions experienced a longer drought propagation time for the year-round. This is particularly true for the upstream and northern downstream regions, with a drought propagation time of more than 11 months. The average drought propagation time in the whole basin reached about 8 months, with the upstream region having the longest propagation time (an average of 12 months), followed by the midstream region (8 months), and the downstream region (6 months) (Fig. 6a).

Figure 6b and c reveals that drought propagation time exhibited seasonal characteristics. More specifically, drought propagated much faster and took less than 2 months to transform from meteorological drought to agricultural drought during the irrigation season in the midstream and downstream regions. In contrast, it lasted for more than 7 months during the non-irrigation season. On average, drought propagation time was shorter during the irrigation season, with an average time of 6 months in the whole basin, and 9, 5, and 3 months in the upstream, midstream, and downstream regions, respectively (Fig. 6b). However, during the non-irrigation season, drought propagation time became longer, with an average time of 10 months in the whole basin, 11 months in both the upstream and midstream regions, and 9 months in the downstream region (Fig. 6c).

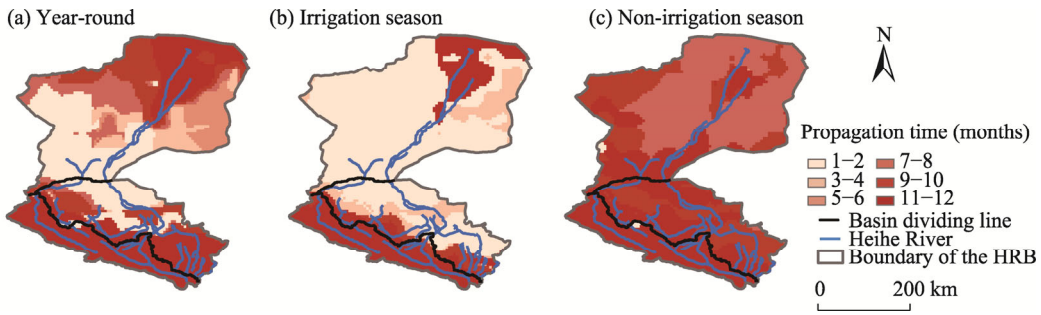

Fig. 6 Spatial distributions of propagation time from meteorological drought to agricultural drought for the year-round (a), and during the irrigation season (b) and non-irrigation season (c) in the HRB

4.2.2 Dynamic characteristics of drought propagation time

To explore the dynamic characteristics of drought propagation time, we set a sliding window of 20 a and divided the study period (1981–2020) into 21 time series. Following this, the trend of drought propagation time in each grid was detected using the Sen's slope estimator and Mann-Kendall test. Figure 7 depicts the spatial distribution of the temporal trends for drought propagation time. All tests exceeded the 95% confidence level, indicating that the trends are significant at the 0.05 significance level. The green color indicates the Sen's slope estimator values greater than zero (upward trend), while the red color means the values less than zero (downward trend).

From Figure 7a it can be seen that at the year-round time scale, the upstream and northern downstream regions (red color; accounting for 56% of the basin) exhibited downward trends of drought propagation time. This indicates a shortening of drought propagation time in these regions. The midstream and southern downstream regions (green color; accounting for 44% of the basin) showed upward trends, revealing that drought propagation time was longer in these regions.

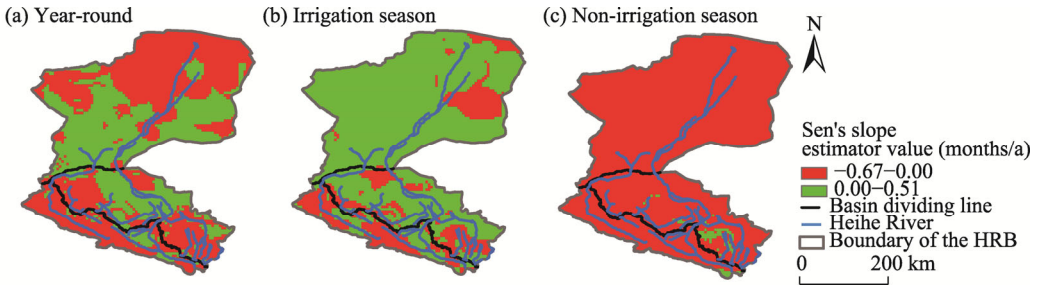

Fig. 7 Spatial distributions of the Sen's slope estimator values (P<0.05) of propagation time from meteorological drought to agricultural drought for the year-round (a), and during the irrigation season (b) and non-irrigation season (c) in the HRB

During the irrigation season, more regions (78% of the basin) presented upward trends (green color in Fig. 7b). However, opposite trends were observed during the non-irrigation season, and nearly 98% of the basin exhibited downward trends (red color in Fig. 7c), indicating that the propagation time from meteorological drought to agricultural drought in most regions of the basin became shorter. More specifically, with the progress of time, agricultural drought triggered by meteorological drought occurred more quickly during the non-irrigation season than during the irrigation season.

4.3 Drought propagation probability

4.3.1 Selection of optimal marginal distribution and copula functions

Drought propagation probability was calculated using the Copula-based interval conditional probability model. The normal, logistic, Weibull, GEV, and P3 marginal distribution functions were used to fit the SPEI and SWDI series. Figure 8 shows the percentage of each marginal distribution function in all grids. GEV ranked the first for the SPEI-1, SPEI-6, and SPEI-12 series (with the percentage values of 64%, 48%, and 54%, respectively) and the second for the SPEI-3 series (with a percentage value of 28%). For SWDI, P3 ranked the first. In order to maintain consistency in selecting an optimal marginal distribution function for each type of drought index, we selected GEV and P3 as the marginal distributions for the SPEI (including SPEI-1, SPEI-3, SPEI-6, and SPEI-12) and SWDI series, respectively.

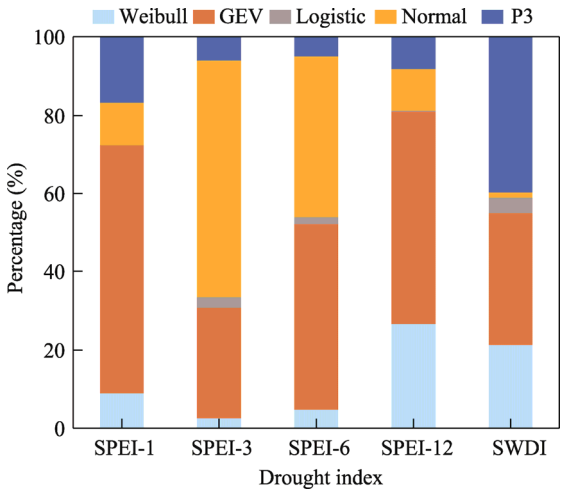

Fig. 8 Percentages of different marginal distribution functions for the SPEI and SWDI series. GEV, General extreme value; P3, Pearson-III.

To ensure the reliability of the selected marginal distribution functions, we also performed the K-S test for each grid. For the SPEI series, more than 94% of the grids can be fitted by GEV, and

for the SWDI series, 82% of the grids can be fitted by P3, according to the K-S test results shown in Table 5. Thus, GEV and P3 were finally determined as the optimal marginal distribution functions for the SPEI and SWDI series, respectively.

Table 5 Percentages of grids that passed the Kolmogorov-Smirnov (K-S) test for the optimal marginal distribution function

Drought index	Optimal marginal distribution function	Percentage of grids that passed the K-S test (%)
SPEI-1	GEV	99.95
SPEI-3	GEV	99.98
SPEI-6	GEV	98.13
SPEI-12	GEV	94.07
SWDI	P3	81.98

Note: GEV, General extreme value; P3, Pearson-III.

The Copula functions were fitted using R (v.4.1.1) (R Development Core Team, 2022), and the function with the largest percentage among all grids was selected as the optimal one. Figures 9 and 10 show the percentage of each Copula function under the AIC and BIC. The Clayton Copula function (light pink in Fig. 9 and green color in Fig. 10) accounted for the highest percentage for the combinations of SPEI-1-SWDI, SPEI-3-SWDI, and SPEI-6-SWDI, and the second-highest percentage for SPEI-12-SWDI (slightly inferior to the Gumbel Copula function). Thus, the Clayton Copula function was finally chosen as the optimal Copula function for the SPEI and SWDI series.

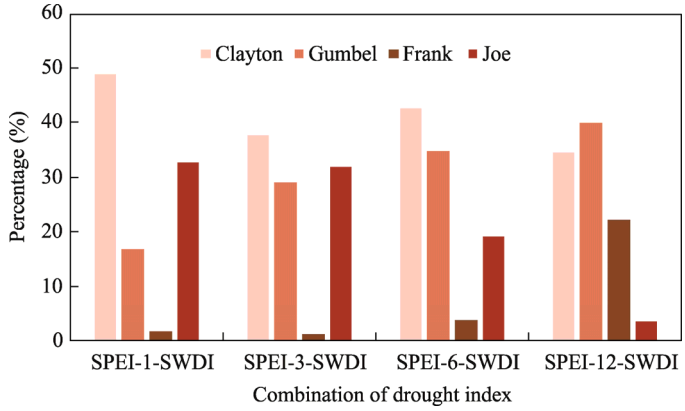

Fig. 9 Percentages of Copula functions for the combinations of SPEI and SWDI series among all grids in the HRB under the Akaike information criterion

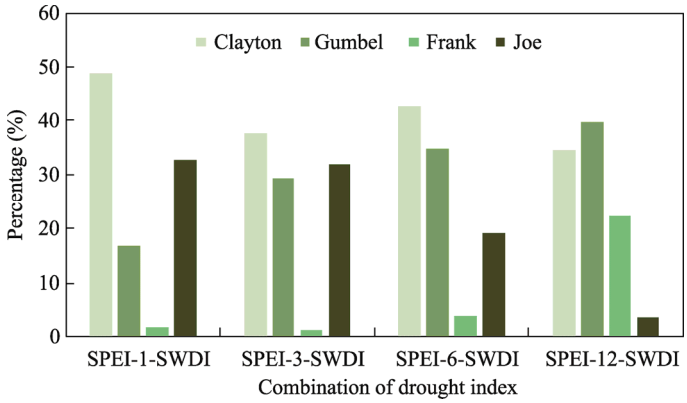

Fig. 10 Percentages of Copula functions for the combinations of SPEI and SWDI series among all grids in the HRB under the Bayesian information criterion

4.3.2 Drought propagation probability and its drought level sensitivity

Drought propagation probability was subsequently calculated using Equations 5 and 6 and the Clayton Copula function. In addition, SPEI-6 was selected to calculate drought propagation probability. This is because the average propagation time from meteorological drought to agricultural drought in the HRB was estimated to be 8 months, which is close to 6 months. In addition, such a medium time scale is suitable for characterizing the propagation of water deficit signals from the atmosphere to the soil (Xu et al., 2021; Yang et al., 2021; Zhang et al., 2021b).

Figure 11 shows the propagation probability of agricultural drought at different levels induced by varying levels of meteorological drought. Drought propagation probability ranged from 0.00 to 1.00, and the redder the color tone, the greater the drought propagation probability value. Generally speaking, agricultural drought caused by meteorological drought exhibited varying spatial trends.

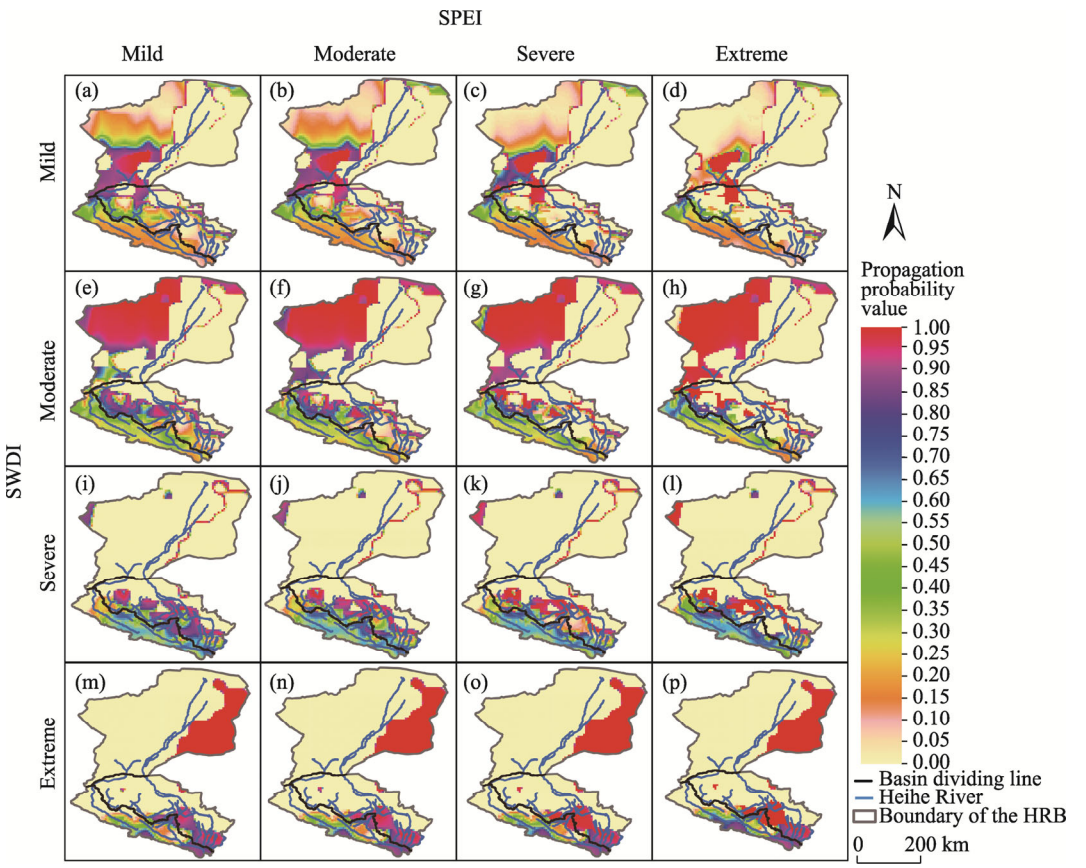

Fig. 11 Spatial distributions of the propagation probability values of different agricultural drought levels (i.e., mild, moderate, severe, and extreme drought levels from the top to bottom) under various meteorological drought levels (i.e., mild, moderate, severe, and extreme drought levels from the left to right) at the year-round scale in the HRB

For the upstream region, when meteorological drought occurred, the propagation probability of severe agricultural drought was about 0.60 (mainly in blue color in Fig. 11i and j), and that of extreme agricultural drought was 0.40–0.85 (green and purple colors in Fig. 11m and n), which was slightly greater than those of mild and moderate agricultural droughts, with the propagation probability values of 0.20 and 0.40 (orange color in Fig. 11a and b for mild agricultural drought, and green color in Fig. 11e and f for moderate agricultural drought). For the eastern upstream region, extreme agricultural drought was more likely to be triggered (Fig. 11m–p), with propagation probability values higher than 0.80. The propagation probability of agricultural

drought at different levels increased with the meteorological drought levels. For example, when the level of meteorological drought increased from moderate to severe, the propagation probability of agricultural drought increased from 0.40 (moderate level) to 0.60 (severe level).

For the midstream region, the propagation probability of agricultural drought at different levels also increased with the meteorological drought levels. For example, the propagation probability of severe agricultural drought increased from 0.80 to over 0.90 when the meteorological drought was from moderate level to severe level (mainly from purple to red color in Fig. 11j and k). For the upstream-midstream junction region, severe and moderate agricultural drought was more likely to occur (Fig. 11e–l), with propagation probability values higher than 0.80.

The downstream region was mainly dominated by mild, moderate, and extreme agricultural droughts induced by meteorological drought. Extreme drought was most likely to occur in the east of the river system (Fig. 11m–p), while moderate agricultural drought was more probable in the west of the river system, with propagation probability values greater than 0.90 (Fig. 11e–h). For the southern downstream region (near the midstream region), the propagation probability of mild and moderate agricultural droughts increased with the meteorological drought levels. For example, the propagation probability of moderate agricultural drought increased from 0.40 to 0.80 and subsequently exceed 0.90 when the meteorological drought increased from the mild level to moderate level and then to the extreme level (Fig. 11e–h). Note that the propagation probability values near the river system were extremely close to zero. This is because soil moisture near the mainstream region was always high, implying that the propagation probability of agricultural drought tends to be low.

In short, with the exceptions of regions close to the river, different agricultural drought levels in the HRB were sensitive to different meteorological drought levels, and such sensitivity exhibited noticeable spatial differences.

4.3.3 Seasonal sensitivity of drought propagation probability

Figures 12 and 13 present the spatial distributions of the seasonal sensitivity of drought propagation probability over the basin. Meteorological drought was more likely to trigger agricultural drought at low levels during the irrigation season and at severe level during the non-irrigation season. Such seasonal sensitivity of drought propagation probability also had noticeable spatial differences.

In particular, for the western downstream region, only mild and moderate agricultural droughts were triggered with the propagation probability values of 0.20–0.40 and >0.90 during the irrigation season, respectively (Fig. 12a–h), while moderate and severe agricultural droughts were triggered during the non-irrigation season, with both propagation probability values higher than 0.85 (Fig. 13a–h). For the southern downstream region, only mild agricultural drought was triggered, with propagation probability values over 0.90 during the irrigation season (Fig. 12a–d), while mild and moderate agricultural droughts were triggered during the non-irrigation season, with propagation probability values greater than 0.85 (Fig. 13a–d). For the eastern downstream region, extreme agricultural drought was most likely to occur with propagation probability exceeding 0.90 regardless of the irrigation and non-irrigation seasons.

For the midstream region, mild, moderate, severe, and extreme agricultural droughts (probability values ranging from 0.20 to higher than 0.90) occurred during both the irrigation and non-irrigation seasons. However, the area of severe agricultural drought triggered during the non-irrigation season was larger than that during the irrigation season (Figs. 12i–l and 13i–l). As for the upstream region, minimal changes were detected for the propagation probability of agricultural drought with varying levels during both the irrigation and non-irrigation seasons (Figs. 12i–l and 13i–l).

5 Discussion

It is well known that there is a water and energy link between meteorological drought and

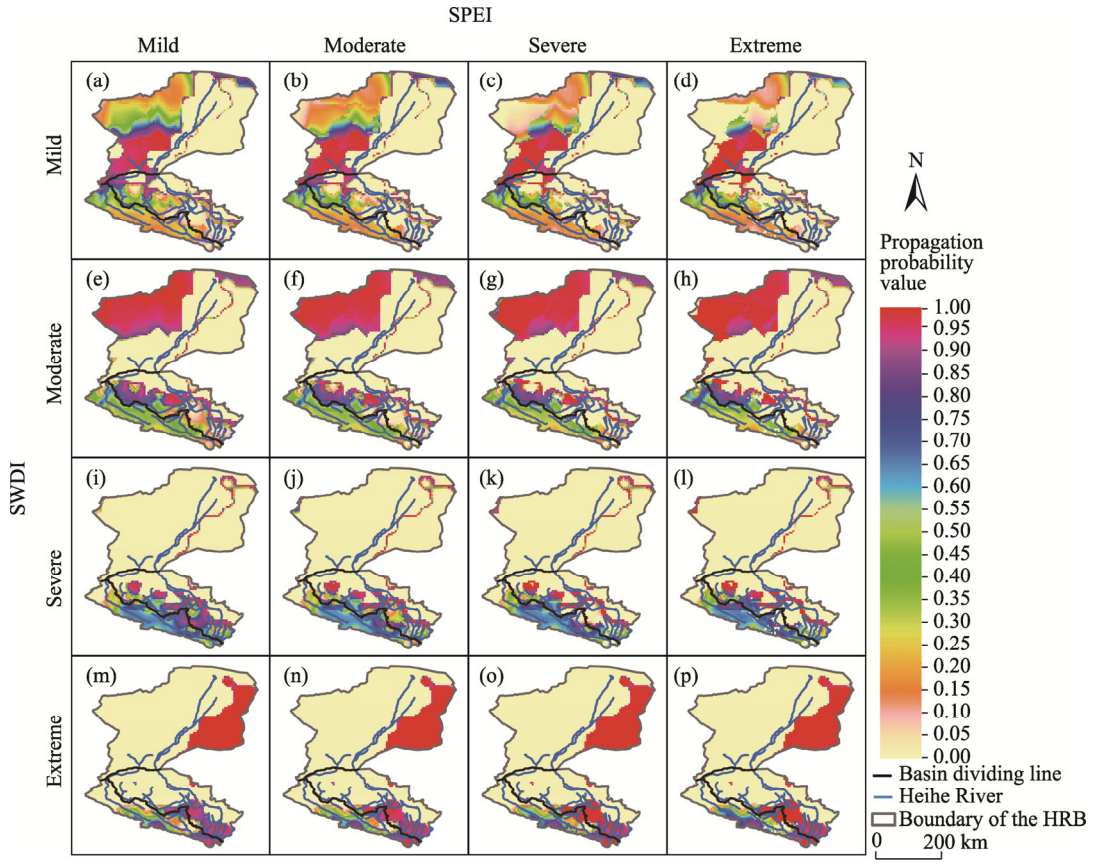

Fig. 12 Spatial distributions of the propagation probability values of different agricultural drought levels (i.e., mild, moderate, severe, and extreme drought levels from the top to bottom) under various meteorological drought levels (i.e., mild, moderate, severe, and extreme drought levels from the left to right) during the irrigation season in the HRB

agricultural drought, with a phase difference in time. The propagation between them is inseparable from the water cycle (Xu et al., 2021; Li et al., 2022). In this study, we analyzed the propagation time and propagation probability from meteorological drought to agricultural drought, as well as their sensitivities to seasons and drought levels in the HRB. The drought propagation characteristics and corresponding sensitivities exhibited great spatial differences, which may be related to the local climate, topography, vegetation cover, etc. (Xu et al., 2019; Zhou et al., 2021a; Zhu et al., 2021; Zhang et al., 2022b).

5.1 Drought propagation time

The upstream region in the HRB was observed to experience a longer propagation time from meteorological drought to agricultural drought, which is probably related to the land use and land cover type. As shown in Figure 3d, the upstream region is mainly covered by forest vegetation, which has a good water holding capacity. In the short term, changes in precipitation have a limited effect on soil moisture. This can result in a slow response of agricultural drought to short term precipitation changes, and thus a longer propagation time from meteorological drought to agricultural drought in the upstream region.

In the midstream and southern downstream regions, drought propagation time was only 1–2 months. This may be related to the climate and geographical conditions of these regions. The midstream of the basin is an agricultural planting region that requires a lot of irrigation water to maintain soil moisture and ensure crop growth. The southern downstream region is dominated by marshland, saline land, and desert, and soil moisture is relatively low, making it particularly

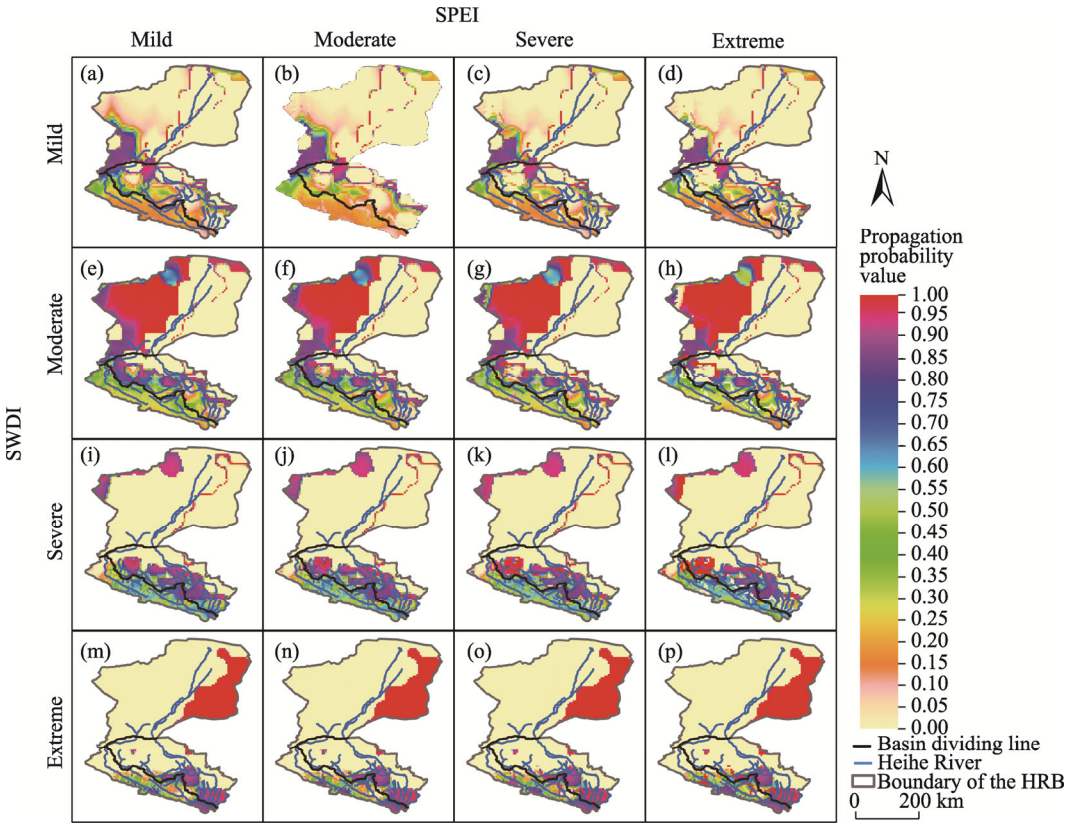

Fig. 13 Spatial distributions of the propagation probability values of different agricultural drought levels (mild, moderate, severe, and extreme drought levels from the top to bottom) under various meteorological drought levels (i.e., mild, moderate, severe, and extreme drought levels from the left to right) during the non-irrigation season in the HRB

important for precipitation to replenish soil moisture. Thus, these regions are more sensitive to changes in climatic conditions. If precipitation continues to be scarce (without considering the artificial diversion irrigation), the soil moisture will be reduced, thus quickening the response of agricultural drought (characterized by soil moisture) to meteorological drought. The northern downstream region contains an inland lake and grassland, where soil moisture is relatively high. Furthermore, the average annual precipitation in this region is minimal (less than 50.0 mm) (Ding et al., 2009; Yang et al., 2022). These may lead to a weak sensitivity of this region to the changes in climatic conditions and thus a slow response of agricultural drought to meteorological drought. Other factors, including wind, radiation, and altitude, could also affect soil moisture availability by influencing evapotranspiration and runoff processes (Van den Hoof and Lambert, 2016).

In the HRB, the irrigation season tends to experience a shorter propagation time from meteorological drought to agricultural drought than the non-irrigation season. This indicates that agricultural drought is more sensitive to meteorological drought during the irrigation season. More than 70% of precipitation is concentrated in June–September (during the irrigation season), and if the lack of precipitation continues to occur, the soil moisture will decrease accordingly. In addition, the period from June to August is the growing season and vegetation growth requires more water from the soil (Qian et al., 2016). Agricultural drought is more likely to be triggered by the lack of precipitation and high-water demand for vegetation growth. Thus, there is a relatively shorter drought propagation time during the irrigation season.

Figure 6b and c reveals that, irrespective of the irrigation or non-irrigation season, the upstream region always experienced a longer drought propagation time compared to other regions of the basin. This may be because the upstream region is dominated by forest, and the roots of the

vegetation are deep and well developed, thus leading to higher resistance to the reduction of surface soil moisture compared to crops, grassland, and marshland covered in the midstream and downstream regions. Moreover, drought propagation time during the irrigation season in the upstream region was slightly shorter than that during the non-irrigation season, which may be due to the presence of snow and ice cover in the basin (Chen et al., 2018; Li et al., 2021). As temperatures increase, snow and permafrost continue to melt, replenishing soil moisture (LYU et al., 2020) and thus shortening drought propagation time during the irrigation season.

Although few studies have investigated the seasonal sensitivity of propagation time from meteorological drought to agricultural drought over the HRB, the relevant cases in other basins can provide reference for us (e.g., Huang et al., 2015; Bhardwaj et al., 2020; Li et al., 2022). For example, Huang et al. (2015) concluded that the propagation time from meteorological drought to agricultural drought in the Weihe River Basin is shorter in summer, and longer in autumn. Liang et al. (2021) estimated that the propagation time from meteorological drought to agricultural drought in the Jinta River Basin of Northwest China was concentrated in 2 months during summer, and 6–12 months in autumn and winter. Li et al. (2022) found that the propagation time from meteorological drought to agricultural drought was shorter (1–3 months) in summer and autumn while longer (5–12 months) in spring and winter over an arid region of Northeast Asia. The previous literature shows that the propagation time from meteorological drought to agricultural drought in summer is relatively shorter, which is similar to our findings in the HRB during the irrigation season.

5.2 Drought propagation probability

The propagation probability of agricultural drought at different levels increased with the meteorological drought levels in the upstream and midstream regions of the HRB. This may be related to the vegetation cover and evapotranspiration. When mild meteorological drought occurs, the excellent water retention capacity of the vegetation can withstand the effects of meteorological drought. However, an extremely reduction in precipitation can induce a water-stressed state of the vegetation, consuming more water through evapotranspiration during droughts, which may exacerbate droughts and induce a higher propagation probability of agricultural drought (Zhu et al., 2021). The propagation probability of agricultural drought triggered by meteorological drought in the midstream region was always higher than that in the upstream region, which is probably due to the different vegetation cover types. The forest in the upstream region can be more drought tolerant because the well-developed root systems can absorb water from deeper soils, while grasses and crops in the midstream region have shorter and undeveloped root systems, which require more shallow soil water to support the growth of them (Zhou et al., 2021a). For the downstream region, the levels of agricultural drought varied at the spatial scale, which was inferred to be largely related to soil moisture. The low soil moisture in the western and eastern downstream region increased the propagation probability of moderate and extreme agricultural droughts, while the high soil moisture near the river system resulted in agricultural drought less likely to be triggered by meteorological drought.

At the seasonal scale, lesser agricultural droughts were more likely to occur during the irrigation season in the midstream and downstream regions, while severer agricultural droughts mostly occurred during the non-irrigation season. This implies that irrigation-induced soil moisture increases could delay and mitigate the effects of meteorological drought on agricultural drought. Irrigation affects the water and energy balance near the ground, making the atmosphere wetter near the surface (Zhu et al., 2021). Therefore, it is speculated that the same level of meteorological drought is more likely to trigger a lower level of agricultural drought during the irrigation season. This result is in agreement with the findings of Fang et al. (2019). In contrast, no obvious differences of propagation probability were observed in the upstream region for both the irrigation and non-irrigation seasons (Figs. 12 and 13) since soil moisture in the upstream region was not affected by irrigation.

6 Conclusions

This study investigated the propagation time and propagation probability from meteorological drought to agricultural drought in the HRB from 1981 to 2020, together with their spatial variations and sensitivities to seasons and drought levels. The correlation coefficient method and Copula-based interval conditional probability model were employed for the analysis. The following conclusions can be drawn from this study.

(1) Larger SPEI values were observed based on SPEI-1, while smaller SPEI values were observed based on SPEI-3, SPEI-6, and SPEI-12. Spatially, smaller SPEI values occurred in the midstream and northern downstream regions. Agricultural drought characterized by SWDI exhibited the most serious level in the eastern downstream region, followed by the upstream region.

(2) The average drought propagation time was estimated to be 8 months in the whole basin at the year-round scale, 6 months during the irrigation season, and 10 months during the non-irrigation season. Drought propagation time had obvious spatial differences in the HRB. By analyzing its dynamic characteristics, we found an increasing trend in 78% of the basin during the irrigation season, and a decreasing trend in 98% of the basin during the non-irrigation season.

(3) Propagation probability was sensitive to seasons and drought levels, and such sensitivity had noticeable spatial differences in the whole basin. In the upstream, midstream, and southern downstream regions, the propagation probability of agricultural drought at different levels increased with the meteorological drought levels. For the western and eastern downstream region, moderate and extreme agricultural droughts were detected to be more easily triggered by meteorological drought, with propagation probability values higher than 0.90. In terms of seasonal sensitivity, lesser agricultural droughts were more likely to be triggered by meteorological drought during the irrigation season, while severer agricultural droughts were occurred mostly during the non-irrigation season.

The results can help to improve our understanding of drought propagation among different drought types, and can act as a useful reference for monitoring meteorological drought and agricultural drought and the rational use of water resources in the HRB. However, this study also has some limitations. For example, the influencing factors of drought propagation characteristics were only explained through qualitative analysis. Quantitative analysis of climate, land use, soil moisture, and irrigation on drought propagation will be the focus of the future work.

Acknowledgements

This study was supported by the National Natural Science Foundation of China (41101038) and the Belt and Road Special Foundation of the State Key Laboratory of Hydrology-Water Resources and Hydraulic Engineering (2021nkms03). We thank the editors and anonymous reviewers for their useful suggestions on improving the quality of this article.

References

Abbas A, Waseem M, Ullah W, et al. 2021. Spatiotemporal analysis of meteorological and hydrological droughts and their propagations. Water, 13(16): 2237, doi: 10.3390/w13162237.

Apurv T, Sivapalan M, Cai X M. 2017. Understanding the role of climate characteristics in drought propagation. Water Resources Research, 53(11): 9304–9329.

Bai J Y, Cui Q, Chen D Q, et al. 2018. Assessment of the SMAP-Derived soil water deficit index (SWDI-SMAP) as an agricultural drought index in China. Remote Sensing, 10(8): 1302, doi: 10.3390/rs10081302.

Bayer Altin T, Altin B N. 2021. Response of hydrological drought to meteorological drought in the eastern Mediterranean Basin of Turkey. Journal of Arid Land, 13(5): 470–486.

Bazrafshan J. 2017. Effect of air temperature on historical trend of long-term droughts in different climates of Iran. Water Resources Management, 31: 4683–4698.

Bhardwaj K, Shah D, Aadhar S, et al. 2020. Propagation of meteorological to hydrological droughts in India. Journal of Geophysical Research: Atmospheres, 125(22): e2020JD033455, doi: 10.1029/2020JD033455.

Chen R, Wang G, Yang Y, et al. 2018. Effects of cryospheric change on alpine hydrology: combining a model with observations in the upper reaches of the Heihe river, China. Journal of Geophysical Research: Atmosphere, 123(7): 3414–3442.

Cheng L, Jin J L, Li J Q, et al. 2013. Advance in the study of drought frequency analysis. Advances in Water Science, 24(2): 296–302. (in Chinese)

Dahal N M, Xiong D H, Neupane N, et al. 2021. Spatiotemporal analysis of drought variability based on the standardized precipitation evapotranspiration index in the Koshi River Basin, Nepal. Journal of Arid Land, 13(5): 433–454.

Dehghani M, Saghafian B, Zargar M, et al. 2019. Probabilistic hydrological drought index forecasting based on meteorological drought index using Archimedean copulas. Hydrology Research, 50(5): 1230–1250.

Ding R, Wang F C, Wang J, et al. 2009. Analysis on spatial-temporal characteristics of precipitation in Heihe River Basin and forecast evaluation in recent 47 years. Journal of Desert Research, 29(2): 335–341. (in Chinese)

Ding Y B, Gong X L, Xing Z X, et al. 2021. Attribution of meteorological, hydrological and agricultural drought propagation in different climatic regions of China. Agricultural Water Management, 255: 106996, doi: 10.1016/j.agwat.2021.106996.

Fang W, Huang S Z, Huang Q, et al. 2019. Probabilistic assessment of remote sensing-based terrestrial vegetation vulnerability to drought stress of the Loess Plateau in China. Remote Sensing of Environment, 232: 111290, doi: 10.1016/j.rse.2019.111290.

Feng K, Su X L. 2020. Spatiotemporal response characteristics of agricultural drought to meteorological drought from a three-dimensional perspective. Transactions of the Chinese Society of Agricultural Engineering, 36(8): 103–113. (in Chinese)

Gu L, Chen J, Yin J B, et al. 2020. Drought hazard transferability from meteorological to hydrological propagation. Journal of Hydrology, 585: 124761, doi: 10.1016/j.jhydrol.2020.124761.

Guo Y, Huang S Z, Huang Q, et al. 2020. Propagation thresholds of meteorological drought for triggering hydrological drought at various levels. Science of The Total Environment, 712: 136502, doi: 10.1016/j.scitotenv.2020.136502.

Heim R R. 2002. A review of twentieth-century drought indices used in the United States. Bulletin of the American Meteorological Society, 83(8): 1149–1166.

Huang S Z, Huang Q, Chang J X, et al. 2015. The response of agricultural drought to meteorological drought and the influencing factors: A case study in the Wei River Basin, China. Agricultural Water Management, 159: 45–54.

Huang S Z, Li P, Huang Q, et al. 2017. The propagation from meteorological to hydrological drought and its potential influence factors. Journal of Hydrology, 547: 184–195.

Jehanzaib M, Kim T W. 2020. Exploring the influence of climate change-induced drought propagation on wetlands. Ecological Engineering, 149: 105799, doi: 10.1016/j.ecoleng.2020.105799.

Li C, Zhang X, Yin G D, et al. 2022. Evaluation of drought propagation characteristics and influencing factors in an arid region of Northeast Asia (ARNA). Remote Sensing, 14(14): 3307, doi: 10.3390/rs14143307.

Li Q F, He P F, He Y C, et al. 2020. Investigation to the relation between meteorological drought and hydrological drought in the upper Shaying River Basin using wavelet analysis. Atmospheric Research, 234: 104743, doi: 10.1016/j.atmosres.2019.104743.

Li X, Zhang L, Zheng Y, et al. 2021. Novel hybrid coupling of ecohydrology and socio-economy at river basin scale: A watershed system model for the Heihe River basin. Environmental Modelling and Software, 141: 105058, doi: 10.1016/j.envsoft.2021.105058.

Li Y G, He J N, Li X. 2016. Evolution of meteorological and hydrological drought in Yunnan Red River Basin based on SPEI and SDI indices analysis. Advances in Geosciences, 35(6): 758–767. (in Chinese)

Liang Z, Su X L, Feng K. 2021. Drought propagation and construction of a comprehensive drought index based on the Soil and Water Assessment Tool (SWAT) and empirical Kendall distribution function ($K_{C'}$): a case study for the Jinta River basin in northwestern China. Natural Hazards and Earth System Sciences, 21(4): 1323–1335.

Liu J, Chai L N, Dong J Z, et al. 2021a. Uncertainty analysis of eleven multisource soil moisture products in the third pole environment based on the three-corned hat method. Remote Sensing of Environment, 255: 112225, doi: 10.1016/j.rse.2020.112225.

Liu L, Niu Q K, Heng J X, et al. 2019. Transition characteristics of the dry-wet regime and vegetation dynamic responses over the Yarlung Zangbo River Basin, Southeast Qinghai-Tibet Plateau. Remote Sensing, 11(10): 1254, doi: 10.3390/rs11101254.

Liu X F, Zhu X F, Pan Y Z, et al. 2018. Performance of different drought indices for agriculture drought in the North China Plain. Journal of Arid Land, 10(4): 507–516.

Liu Y J, Huang S Z, Fang W, et al. 2021b. Propagation and dynamic change of meteorological drought to hydrological drought in different seasons. Journal of Hydraulic Engineering, 52(1): 93–102. (in Chinese)

LYU M X, Wang Y B, Liu G H. 2020.Changes in shallow soil moisture and its influencing factors in the alpine region of the upper Heihe River. Arid Zone Research, 37(4): 899–907. (in Chinese)

Martínez-Fernández J, González-Zamora A, Sánchez N, et al. 2015. A soil water based index as a suitable agricultural drought indicator. Journal of Hydrology, 522: 265–273.

Ministry of Agriculture of the People's Republic of China. 2017. Current Land Use Classification (GB/T 21010-2017). [S/OL]. [2023-02-28]. https://openstd.samr.gov.cn/bzgk/gb/newGbInfo?hcno=224BF9DA69F053DA22AC758AAAADEEAA.

Mishra A K, Singh V P. 2012. A review of drought concepts. Journal of Hydrology, 391(1–2): 202–216.

Moral F J, Paniagua L L, Rebollo F J, et al. 2017. Spatial analysis of the annual and seasonal aridity trends in Extremadura, southwestern Spain. Theoretical and Applied Climatology, 130(3–4): 917–932.

Qian Y Q, He F P, Wang W. 2016. Seasonality, rather than nutrient addition or vegetation types, influenced short-term temperature sensitivity of soil organic carbon decomposition. PloS ONE, 11(4): e0153415, doi: 10.1371/journal.pone.0153415.

R Development Core Team. 2022. R: A language and environment for statistical computing. R foundation for statistical computing, Vienna, Austria. https://cran.r-project.org/bin/windows/base/rpatched.html.

Rodell M, Houser P R, Jambor U, et al. 2004. The global land data assimilation system. Bulletin of the American Meteorological Society, 85(5): 381–394.

Sattar M N, Lee J Y, Shin J Y, et al. 2019. Probabilistic characteristics of drought propagation from meteorological to hydrological drought in South Korea. Water Resources Management, 33: 2439–2452.

Shao S J, Xu G Y, Li M, et al. 2019. Synchronizing e-commerce city logistics with sliding time windows. Transportation Research Part E: Logistics and Transportation Review, 123: 17–28.

Shin J Y, Chen S, Lee J H, et al. 2018. Investigation of drought propagation in South Korea using drought index and conditional probability. Terrestrial Atmospheric and Oceanic Sciences, 29(2): 231–241.

Sun X. 2021. Study on propagation characteristics of meteorological drought to hydrological drought based on non-stationary index. MSc Thesis. Beijing: China University of Geosciences. (in Chinese)

Um M -J, Kim Y, Jung K, et al. 2022. Evaluation of drought propagations with multiple indices in the Yangtze River basin. Journal of Environmental Management, 317: 115494, doi: 10.1016/j.jenvman.2022.115494.

Van den Hoof C, Lambert F. 2016. Mitigation of drought negative effect on ecosystem productivity by vegetation mixing. Journal of Geophysical Research: Biogeosciences, 121(10): 2667–2683.

Vicente-Serrano S M, Beguería S, López-Moreno J I. 2010. A multiscalar drought index sensitive to global warming: the standardized precipitation evapotranspiration index. Journal of Climate, 23(7): 1696–1718.

Wang F. 2020. Study on the spatial and temporal evolution characteristics of drought in the Yellow River Basin from the perspective of multiple drought types. PhD Dissertation. Zhengzhou: Zhengzhou University. (in Chinese)

Wang J S, Li Y H, Wang R Y, et al. 2012. Preliminary analysis on the demand and review of progress in the field of meteorological drought research. Journal of Arid Meteorology, 30(4): 497–508. (in Chinese)

Wang J. 2019. Simulation and prediction of runoff in the upper reaches of Heihe River Basin under climate change conditions. MSc Thesis. Beijing: China University of Geosciences. (in Chinese)

Wu Z M, Qiu J X, Liu S X, et al. 2020. Advances in agricultural drought monitoring based on soil moisture. Progress in Geography, 39(10): 1758–1769. (in Chinese)

Wu Z Y, Feng H H, He H, et al. 2021. Evaluation of soil moisture climatology and anomaly components derived from ERA5-Land and GLDAS-2.1 in China. Water Resources Management, 35: 629–643.

Xu Y, Zhang X, Wang X, et al. 2019. Propagation from meteorological drought to hydrological drought under the impact of human activities: A case study in northern China. Journal of Hydrology, 579: 124147, doi: 10.1016/j.jhydrol.2019.124147.

Xu Y, Zhang X, Hao Z C, et al. 2021. Characterization of agricultural drought propagation over China based on bivariate probabilistic quantification. Journal of Hydrology, 598: 126194, doi: 10.1016/j.jhydrol.2021.126194.

Yang M K, He Z H, Zhang L, et al. 2021. Propagation process of meteorological drought to hydrological drought in different

time scales. Journal of Soil and Water Conservation, 35(6): 350–360. (in Chinese)

Yang S, Chen K W, Zhu B W, et al. 2022. How does irrigation alter the water, carbon, and nitrogen budgets in a large endorheic river basin? Journal of Hydrology, 613: 128317, doi: 10.1016/j.jhydrol.2022.128317.

Zhang G X, Su X L, Ayantobo O O, et al. 2021a. Drought monitoring and evaluation using ESA CCI and GLDAS-Noah soil moisture datasets across China. Theoretical and Applied Climatology, 144: 1407–1418.

Zhang Q, Shi R, Singh V P, et al. 2022a. Droughts across China: drought factors, prediction and impacts. Science of The Total Environment, 803: 150018, doi: 10.1016/j.scitotenv.2021.150018.

Zhang T, Su X L, Zhang G X, et al. 2022b. Evaluation of the impacts of human activities on propagation from meteorological drought to hydrological drought in the Weihe River Basin, China. Science of The Total Environment, 819: 153030, doi: 10.1016/j.scitotenv.2022.153030.

Zhang Y, Hao Z C, Feng S F, et al. 2021b. Agricultural drought prediction in China based on drought propagation and large-scale drivers. Agricultural Water Management, 255: 107028, doi: 10.1016/j.agwat.2021.107028.

Zhou K K, Li J Z, Zhang T, et al. 2021a. The use of combined soil moisture data to characterize agricultural drought conditions and the relationship among different drought types in China. Agricultural Water Management, 243(1): 106479, doi: 10.1016/j.agwat.2020.106479.

Zhou Z Q, Shi H Y, Fu Q, et al. 2021b. Characteristics of propagation from meteorological drought to hydrological drought in the Pearl River Basin. Journal of Geophysical Research: Atmospheres, 126(4): e2020JD033959, doi: 10.1029/2020jd033959.

Zhu Q, Luo Y L, Xu Y P, et al. 2019. Satellite soil moisture for agricultural drought monitoring: assessment of SMAP-derived soil water deficit index in Xiang River Basin, China. Remote Sensing, 11(3): 362, doi: 10.3390/rs11030362.

Zhu Y, Liu Y, Wang W, et al. 2021. A global perspective on the probability of propagation of drought: from meteorological to soil moisture. Journal of Hydrology, 603: 126907, doi: 10.1016/j.jhydrol.2021.126907.